



HAL
open science

Solid-state [^{13}C - ^{15}N] NMR resonance assignment of hepatitis B virus core protein

Lauriane Lecoq, Shishan Wang, Thomas Wiegand, Stéphane Bressanelli,
Michael Nassal, Beat H Meier, Anja Böckmann

► **To cite this version:**

Lauriane Lecoq, Shishan Wang, Thomas Wiegand, Stéphane Bressanelli, Michael Nassal, et al.. Solid-state [^{13}C - ^{15}N] NMR resonance assignment of hepatitis B virus core protein. *Biomolecular NMR Assignments*, 2018, 12 (1), pp.205-214. 10.1007/s12104-018-9810-y . hal-02022693

HAL Id: hal-02022693

<https://hal.science/hal-02022693>

Submitted on 18 Feb 2019

HAL is a multi-disciplinary open access archive for the deposit and dissemination of scientific research documents, whether they are published or not. The documents may come from teaching and research institutions in France or abroad, or from public or private research centers.

L'archive ouverte pluridisciplinaire **HAL**, est destinée au dépôt et à la diffusion de documents scientifiques de niveau recherche, publiés ou non, émanant des établissements d'enseignement et de recherche français ou étrangers, des laboratoires publics ou privés.

[Click here to view linked References](#)

Solid-state [^{13}C - ^{15}N] NMR resonance assignment of hepatitis B virus core protein

Lauriane Lecoq⁺ · Shishan Wang⁺ · Thomas Wiegand · Stéphane Bressanelli · Michael Nassal ·
Beat H. Meier · Anja Böckmann

⁺ Lauriane Lecoq and Shishan Wang have contributed equally to this work.

Affiliations:

L. Lecoq · S. Wang · A. Böckmann

Institut de Biologie et Chimie des Protéines, Bases Moléculaires et Structurales des Systèmes
Infectieux, Labex Ecofect, UMR 5086 CNRS, Université de Lyon, 7 passage du Vercors,
69367 Lyon, France

Thomas Wiegand · B. H. Meier

Physical Chemistry, ETH Zurich, 8093 Zurich, Switzerland

S. Bressanelli

Institute for Integrative Biology of the Cell (I2BC), CEA, CNRS, Univ Paris Sud, Université
Paris-Saclay, 91198, Gif sur Yvette cedex, France

M. Nassal

University Hospital Freiburg, Department of Internal Medicine II / Molecular Biology,,
Hugstetter Straße 55, 79106 Freiburg, Germany

Corresponding authors

Anja Böckmann: a.boeckmann@ibcp.fr

Beat H. Meier: beme@ethz.ch

Michael Nassal: michael.nassal@uniklinik-freiburg.de

Abstract

Each year, nearly 900,000 deaths are due to serious liver diseases caused by chronic hepatitis B virus (HBV) infection. The viral particle is composed of an outer envelope and an inner icosahedral nucleocapsid formed by multiple dimers of a ~20 kDa self-assembling core protein (Cp). Here we report the solid-state ^{13}C and ^{15}N resonance assignments of the assembly domain, Cp149, of the core protein in its capsid form. A secondary chemical shift analysis of the 140 visible residues suggests an overall alpha-helical three-dimensional fold matching that derived for Cp149 from the X-ray crystallography of the capsid, and from solution-state NMR of the Cp149 dimer. Interestingly, however, at three distinct regions the chemical shifts in solution differ significantly between core proteins in the capsid state versus in the dimer state, strongly suggesting the respective residues to be involved in capsid assembly.

Keywords:

Hepatitis B virus · Core protein · Nucleocapsid · Solid-state NMR · Assignments

Biological Context

1
2
3 More than 2 billion people have been infected with hepatitis B virus (HBV), and more than
4
5 250 million thereof have become chronic carriers of the virus. Each year, close to 900,000
6
7 people die from hepatitis B as they develop chronic liver disease, including cancer (World
8
9 Health Organization 2017). While an effective prophylactic vaccine is available to prevent
10
11 infection, current treatments for chronic HBV infection are rarely curative and subject to the
12
13 emergence of resistant virus variants (Zoulim and Durantel 2015). Hence new therapeutic
14
15 options are urgently sought (Revill et al. 2016).
16
17

18
19 The HBV virus particle (virion) is composed of an outer envelope bearing three related
20
21 surface antigen (HBsAg) proteins and an inner nucleocapsid formed by multiple copies of a
22
23 single about 20 kDa core protein (Cp) species. Cp forms stable dimers capable of self-
24
25 assembling the capsid shell. The predominant form consists of 120 Cp dimers arranged
26
27 in T=4 icosahedral symmetry. In infection, newly forming nucleocapsids initially co-
28
29 package a complex of one copy of the viral pregenomic (pg) RNA plus one copy of the viral
30
31 polymerase (Pol); maturation involves capsid-assisted reverse transcription of the pgRNA into
32
33 a relaxed circular DNA by Pol (Nassal 2015). The N terminal ~140 amino-acids of Cp,
34
35 modeled by C terminally truncated variants like Cp149, are required and sufficient for capsid
36
37 shell formation, even in bacteria (Gallina et al. 1989; Birnbaum and Nassal 1990). The
38
39 downstream arginine-rich C-terminal domain (CTD) generally binds nucleic acids (Birnbaum
40
41 and Nassal 1990) but is also required for specific viral pgRNA packaging (Nassal 1992). 3D
42
43 structures, first by cryo-electron microscopy (EM) reconstruction, revealed mostly an α -
44
45 helical fold (Conway et al. 1997; Böttcher et al. 1997). The crystallographic structure of
46
47 Cp149 later solved at a resolution of 3.3 Å (Wynne et al. 1999) gave an atomic-level view of
48
49 the protein. Since then, further structures of the HBV capsid have been solved either by cryo-
50
51 EM (Crowther et al. 1994; Dryden et al. 2006; Chen et al. 2011; Yu et al. 2013; Selzer et al.
52
53
54
55
56
57
58
59
60
61
62
63
64
65

1 2015; Patel et al. 2017) or crystallography (Bourne et al. 2006; Katen et al. 2013). Yet,
2 despite these structural studies, many steps along the viral life cycle involving the core protein
3
4 are not yet fully understood; namely, as the conformation of the capsids is believed to be a
5
6 function of the different maturation states (Ning et al. 2017), it is central to structurally
7
8 analyze the capsids under a larger variety of conditions. In this context, solid-state NMR is an
9
10 attractive technique since it allows the study of large molecular assemblies as viral capsids at
11
12 physiological temperature, including those not forming crystalline states, which enables the
13
14 study of different constructs, formed in various environments. First applications of solid-state
15
16 NMR to virus capsids have been described in the literature and made significant advances in
17
18 the understanding of different viral cycles. For example, Polenova and coworkers have
19
20 determined a structural model of the human immunodeficiency virus 1 (HIV-1) capsids and
21
22 have shown that the internal flexibility of the capsid protein is essential for its assembly and
23
24 interaction with host partners (Han et al. 2010; Quinn et al. 2015; Suiter et al. 2015). Solid-
25
26 state NMR also allowed the characterization of the dynamics of fd bacteriophage, both of the
27
28 filamentous and icosahedral, as well as to probe the capsid regions involved in the interaction
29
30 with the DNA genome of the virus (Morag et al. 2014; Abramov et al. 2015). More recently,
31
32 the structure of the *Acinetobacter* phage 205 has been solved (Andreas et al. 2016) using the
33
34 advances in NMR technology with faster spinning frequencies (110 kHz) and ^1H detection
35
36 techniques (Penzel et al. 2015; Stanek et al. 2016). All these studies have paved the way
37
38 towards the analysis of a large variety of viral capsid assemblies using magic-angle spinning
39
40 (MAS)-NMR, in order to understand the viral life cycle.

41
42 Here we report the ^{13}C and ^{15}N resonance assignments of the HBV core protein Cp149 in the
43
44 capsid form as assembled in *E. coli* using 2D and 3D solid-state NMR experiments. The
45
46 spectra obtained show narrow lines (between 70 and 100 Hz in ^{13}C) typical for highly ordered
47
48 assemblies. We compare the obtained chemical shifts and secondary structures to previous
49
50

1 structural studies by X-ray and solution-state NMR, and highlight that the differences are
2 mainly located at the dimer interfaces. This assignment of the assembly domain forms the
3 first step towards investigation of full-length Cp183 particles, either filled with RNA, or
4 mostly devoid of RNA upon extensive phosphorylation of the C-terminal domain.
5
6
7
8
9

10 **Materials and methods**

11 **Protein expression and purification; sample preparation**

12 Cp149 was expressed and purified as described previously (Heger-Stevic et al. 2017). Briefly,
13 the pET-28a2-Cp149opt plasmid was transformed into *E.coli* BL21* Codon + (DE3) cells and
14 grown at 37 °C overnight on a LB-agar plate containing 100 µg/ml ampicillin and 34 µg/ml
15 chloramphenicol. Then, a single colony was inoculated into 3 ml LB medium and grown at 37
16 °C for 5 h. It was then transferred into 50 ml of standard M9 minimal medium containing
17 ¹⁵NH₄Cl and ¹³C-glucose as the sole nitrogen and carbon sources. The culture was incubated
18 for 4 hours at 37 °C and transferred into 100 ml fresh ¹³C-¹⁵N M9 medium for an overnight
19 incubation at 25 °C. 850 ml of ¹³C-¹⁵N M9 medium were inoculated with the 150 ml
20 overnight ¹³C-¹⁵N M9 culture. When OD₆₀₀ reached 0.7, the bacterial cells were grown for
21 another 6 h at 25 °C after induction with 1 mM IPTG.
22
23
24
25
26
27
28
29
30
31
32
33
34
35
36
37
38
39

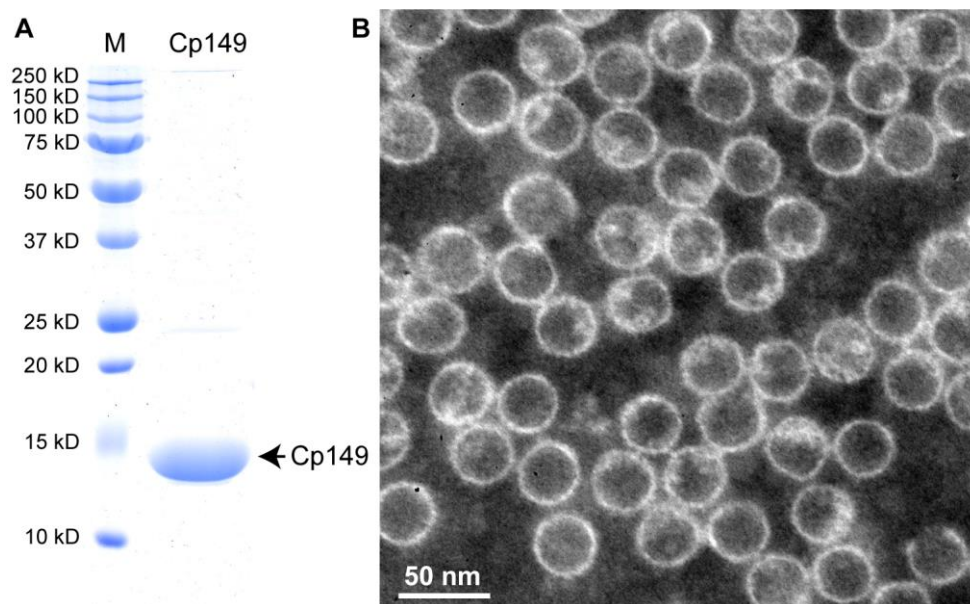
40 Bacterial cells were pelleted by centrifugation (6,000 g, 20 min) and re-suspended in 15 ml
41 of lysis buffer (50 mM Tris pH 7.4, 300 mM NaCl, 5 mM DTT). 15 mg of chicken lysozyme,
42 300 µl of protease inhibitor cocktail solution 50X and 750 µl of 10% Triton-X-100 was added
43 to the cell suspension and incubated on ice for 45 min. Benzonase nuclease was added to the
44 suspension and mixed for 30 min at room temperature. The cells were lysed by sonication and
45 then centrifuged at 8000 g for 1 h to remove cell debris. The supernatant was loaded onto a
46 step gradient from 10% to 70% (m/v) sucrose (buffered in 50 mM Tris pH 7.5, 300 mM NaCl,
47 5 mM DTT) and centrifuged in SW-32Ti Beckman Coulter rotor at 28,800 g for 3 h at 4 °C.
48 The gradient fractions containing Cp149 capsids were identified by SDS-PAGE (using
49
50
51
52
53
54
55
56
57
58
59
60
61
62
63
64
65

1
2
3
4
5
6
7
8
9
10
11
12
13
14
15
16
17
18
19
20
21
22
23
24
25
26
27
28
29
30
31
32
33
34
35
36
37
38
39
40
41
42
43
44
45
46
47
48
49

Tris/Glycine/SDS buffer from BioRad and 15 % acrylamide) and precipitated by slow addition of $(\text{NH}_4)_2\text{SO}_4$ to 20% saturation. After incubation on ice for 1 h and centrifugation at 25,000 g for 1 h, pellets were resuspended in purification buffer (50 mM Tris pH 7.5, 5 mM EDTA, 5 mM DTT, 5% sucrose). The protein solution was centrifuged again for 15 min to remove insoluble pellets and the supernatant containing soluble capsids was dialyzed overnight in purification buffer at 4 °C.

Electron microscopy

5 μL of sample were loaded on a carbon-coated grid and incubated for 2 minutes. The grid was then layered on top of 50 μL of 2 % phosphotungstic acid (m/v) pH 7 and incubated at room temperature for 2 minutes for negative staining. The grids were examined with a JEM-1400 transmission electron microscope operating at 100 kV.



50
51
52
53
54
55
56

Fig. 1 Sample characterization. A. SDS-PAGE 15% acrylamide of a molecular weight marker (Precision Plus Protein™ Unstained Standards from BioRad) and 20 μg of purified Cp149 expressed in *E. coli*. B. Negative-stain EM picture of Cp149 concentrated at 1 mg/ml.

Solid-state NMR spectroscopy

57
58
59
60
61
62
63
64
65

1 For NMR sample preparation, we started from 40 mg of soluble capsids which were
2 concentrated to a final volume of 1 ml and sedimented into a thin-wall 3.2 mm zirconium rotor
3
4 by centrifugation (180,000 g, 14 h, 4 °C) using a home-made filling tool (Böckmann et al.
5
6 2009). All NMR experiments were conducted using a 3.2 mm triple-resonance (^1H , ^{13}C , ^{15}N)
7
8 probe head at static magnetic field of 18.8 T corresponding to 800 MHz proton resonance
9
10 frequency (Bruker Avance II). Assignments were obtained at a MAS frequency of 17.5 kHz
11
12 using a combination of 2D and 3D correlation experiments, including: 2D DARR, 3D
13
14 NCACB, NCACX, NCOCX, CANCO and CCC (Schuetz et al. 2010; Habenstein et al. 2011).
15
16 The 3D CCC was performed with the probe in double-resonance (^1H , ^{13}C) mode allowing to
17
18 increase the signal to noise ratio by a factor of 1.4. Experimental details are given in Table 1.
19
20
21 All spectra were referenced using DSS and recorded at a sample temperature of 4 °C, as
22
23 determined by the resonance frequency of the supernatant water (Böckmann et al. 2009).
24
25 Two-dimensional DARR, NCA and NCO spectra were recorded on several other preparations
26
27 of the same protein assembly, and resulted in reproducible spectra. Two-dimensional DARR
28
29 and NCA spectra of Cp149 capsids were also recorded at 37 °C to confirm that under
30
31 physiological temperatures, the protein conformation remained identical. Three-dimensional
32
33 spectra were subsequently recorded for 2–6 days each on a single sample of Cp149. Side-
34
35 chain assignments were achieved using NCACB, NCACX, NCOCX and CCC spectra
36
37 (Schuetz et al. 2010; Habenstein et al. 2011). All spectra were processed using TopSpin 3.2
38
39 (Bruker Biospin) by zero filling to no more than double the number of acquired points, the
40
41 time domain signals were apodized with a squared cosine function (SSB 2.5–3 depending on
42
43 spectrum and dimension). Spectra analysis and assignment was done with the CcpNmr
44
45 Analysis package (Vranken et al. 2005; Stevens et al. 2011).
46
47
48
49
50
51
52
53
54
55
56
57

58 **Assignments and data deposition**

59
60
61
62
63
64
65

Sequential assignments and secondary chemical shifts

¹³C and ¹⁵N backbone and side-chain chemical shifts of the Cp149 capsid protein have been deposited in the BioMagResBank (<http://www.bmrb.wisc.edu>) under the accession number 27317. Capsids expressed with high yield of minimum 50 mg per liter culture, and final preparations showed a high purity level as shown in Figure 1A. Purified proteins were analyzed under the electron microscope. As described previously (Birnbaum and Nassal 1990), capsids were assembled directly during bacterial expression, as numerous HBV core protein capsids were observed under the electron microscope (see Figure 1B for negative-stain EM pictures). Capsid preparations were homogenous and showed mainly T=4 capsids with a typical diameter of 30 ± 3 nm. The 2D ¹³C-¹⁵N NCA spectrum of assigned Cp149 capsids is displayed in Figure 2A and shows narrow peaks with full widths at half maximum (FWHM) between 70 and 100 Hz in ¹³C, which is comparable to line widths obtained previously in viral capsid proteins such as the HIV-1 virion (Suiter et al. 2015) and is indicative for homogeneous preparations of uniformly labeled proteins. Representative planes of the 3D NCACB, NCACO, CANCO and NCOCA experiments are shown in Figure 2B. Assignments of Cp149 were completed at 87 % for all backbone atoms, with missing assignments predominantly found at the protein C-terminal end including residues 140 to 149 for which no cross peaks were detected in 3D spectra. In detail, 95.6 % of N, 97.1 % of C α , 97.8 % of C', and 75.3 % of side chain non-H (including 96.2 % of C β) were unambiguously assigned for residues 1–139 of Cp149.

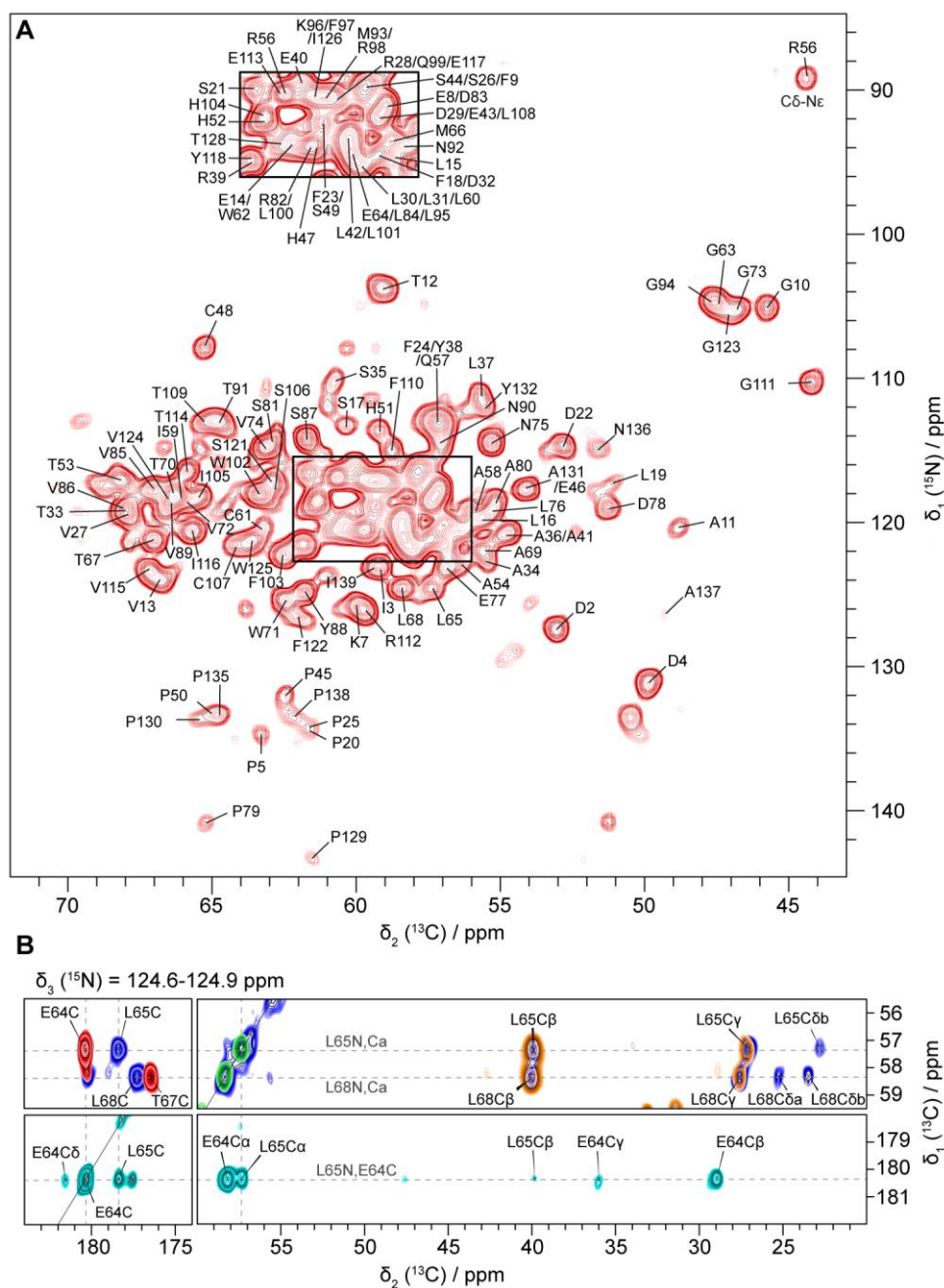


Fig. 2D and 3D spectra used in sequential assignments: **A)** 2D ^{13}C - ^{15}N NCA spectrum of Cp149 capsids. All assigned N-C α intra-residue correlations are labeled with the residue number as well the C α -C δ intra-residue correlations for proline residues. The middle of the spectrum is copied inside the black rectangle for more clarity. **B)** Representative plane for residue Leu65 of 3D CANCO (red), NCACX (dark blue), NCACB (green for positive signals and orange for negative signals) and NCOCX (cyan) spectra. For experimental details see Table 1.

A secondary chemical-shift analysis (Figure 3) reveals a backbone fold similar to that of the X-ray capsid structure as described in (Wynne et al. 1999). Helices $\alpha 1$ (residues 13-17) and

1
2
3
4
5
6
7
8
9
10
11
12
13
14
15
16
17
18
19
20
21
22
23
24
25
26
27
28
29
30
31
32
33
34
35
36
37
38
39
40
41
42
43
44
45
46
47
48
49
50
51
52
53
54
55
56
57
58
59
60
61
62
63
64
65

$\alpha 2$ (residues 27-43) appear to be the same length in both capsids, furthermore the smaller values of secondary chemical shifts obtained for residues 37 and 38 are representative of the 90°-kink observed in the X-ray structure. The two short helical stretches between residues 7-9 and 21-23 described in the x-ray structure file can be identified as one-turn helices spanning 4 residues by NMR. NMR also detects a short β -strand from residues 1 to 4, a stretch which takes an extended conformation in the x-ray structure. Helix $\alpha 3$ (residues 50-76 in solid-state NMR) is predicted to be longer by three residues, while helix $\alpha 5$ is predicted to be two-residues shorter (residues 112-125). Another difference is observed in helix $\alpha 4$ that is not divided into two smaller helices in the NMR predictions but instead would form a continuous 30-amino acids helix, shorter by one residue compared to the X-ray structure. While these differences may be real structural differences between the two capsids analyzed, it is more likely that they are due to the more or less stringent conditions the structure analysis programs put on dihedral angles to identify helical segments. Also, NMR secondary chemical shifts might slightly vary depending on which average chemical shifts are taken as a basis. In both cases small variations can lead to values disregarded, or defined, as helices.

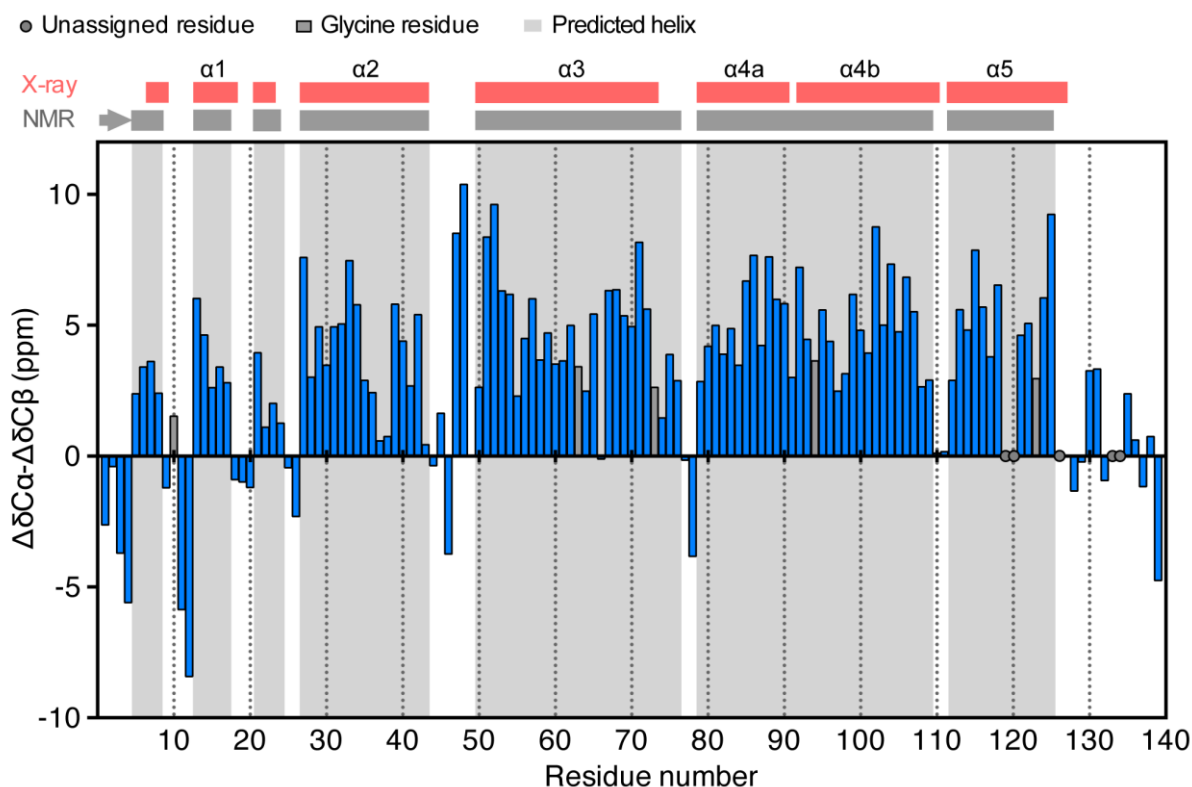


Fig. 3 Differences between secondary chemical shifts of $C\alpha$ and $C\beta$ resonances relative to their random coil shift (Wishart et al. 1995) as a function of Cp149 residue number. Missing assignments are represented as grey circles and include residues L119, V120, I126, R133, P134, as well as the C-terminal end from 140 to 149. For glycine residues (shown as grey bar), the deviation of the $C\alpha$ shift from the random coil value is plotted. The α -helices found in the X-ray structure of Cp149 capsid as described in (Wynne et al. 1999) are shown as pink boxes at the top of the graph and the ones predicted from solid-state NMR chemical shifts are shown as grey boxes. Four residues in a row with a positive value are indicative of an α -helix and three residues in a row with a negative value indicate a β -strand.

Comparison to Cp149 dimer chemical shifts from solution-state NMR

Chemical shifts of the dimeric core protein have previously been determined using solution-state NMR on a protein comprising a slightly different amino-acid sequence (Freund et al. 2008); furthermore, to prevent the dimers from assembling, solution spectra were taken at pH 9.5 and at low salt concentrations. The backbone assignments here presented for the capsid form of Cp149 are slightly more complete than the ones determined for the Cp149 dimer, as conformational exchange likely induced the loss of several signals in the solution-state study. Also, the high pH used in that study might have been responsible for solvent-saturation

1 transfer effects. A comparison between the dimer and capsid chemical shifts is shown in
2 Figure 4A for C α and C β resonances. Chemical shifts of the six residues which were different
3
4 between the two Cp149 constructs used were disregarded (A35, D40, D64, T74, V93 and
5
6 L116 in the solution study). While overall chemical shifts are rather similar between the
7
8 dimer and capsid form, interesting chemical shift differences, which we interpret as chemical-
9
10 shift perturbations (CSPs) upon assembly, are observed in three distinct regions identified in
11
12 Figure 4B. The first region includes residues 18 to 23, which are involved in contacts with
13
14 two different surrounding dimers in the capsid structure. The residues with which they are in
15
16 interaction on the neighboring dimers comprise amino acids 136-138, which however have
17
18 not been assigned for the dimer in solution. Other significant CSPs are observed in a second
19
20 region from residues 55 to 62, which could be due to the different oxidation state of C61, or
21
22 alternatively to allosteric changes induced by the interaction between the dimers in the capsid
23
24 form. These changes could be transmitted via a third region showing CSPs comprising
25
26 residues 96 and 97, which is located in between regions 1 and 2. Met1 also shows an isolated
27
28 CSP, probably due to the close proximity with the second region affected by capsid assembly.
29
30 CSPs observed for residues neighboring residues with different amino acids in the two
31
32 constructs in the sequence, as is the case for residues N75 and L76, were disregarded in our
33
34 analysis as they rather stem from sequence differences than to differences caused by
35
36 assembly. Our results reveal the three major regions undergoing a conformational change
37
38 between the core protein in solution and the core protein assembled as a capsid.
39
40
41
42
43
44
45
46
47
48
49
50
51
52
53
54
55
56
57
58
59
60
61
62
63
64
65

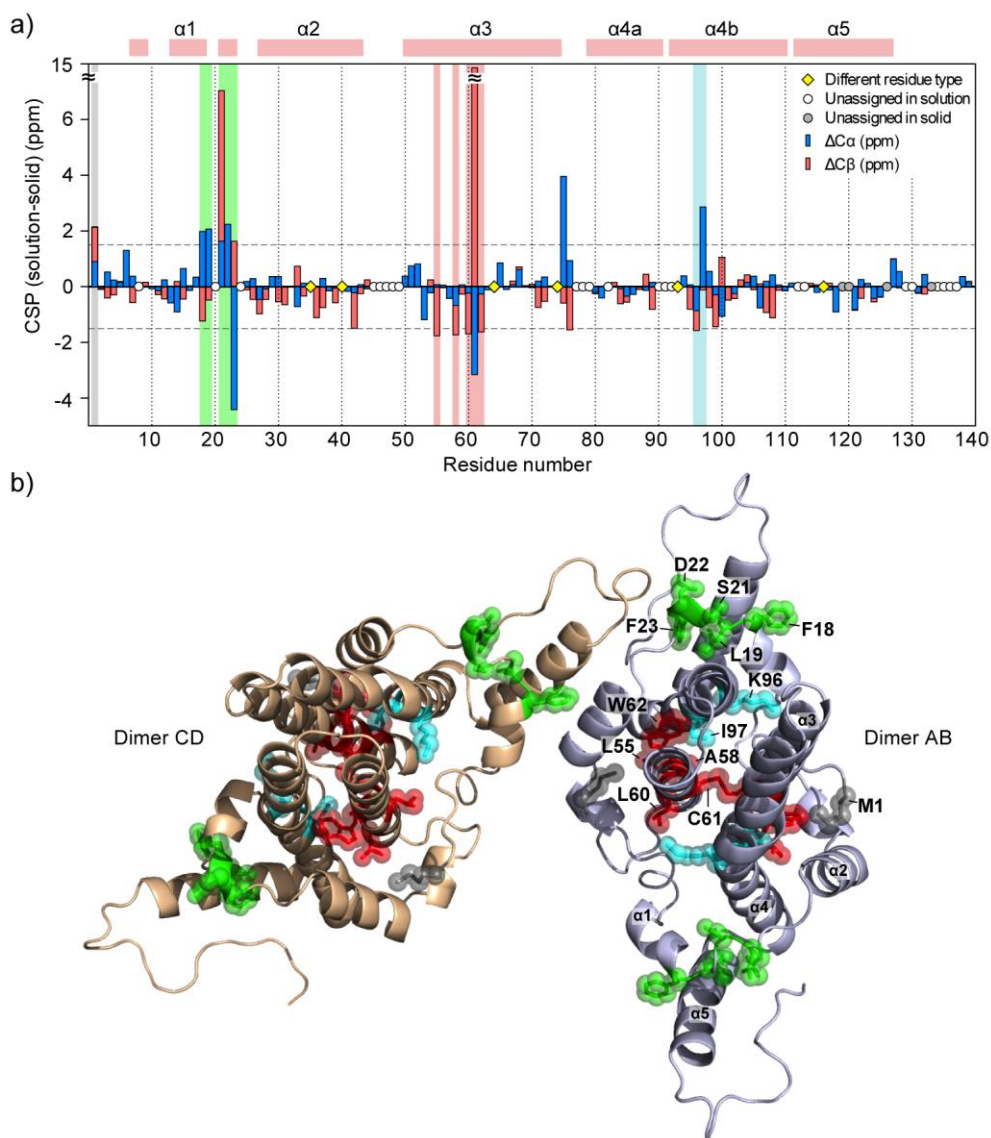


Fig. 4 Chemical shift perturbations between dimeric Cp149 and Cp149 capsids. CSP from $C\alpha$ resonances are shown in blue and $C\beta$ in red. Yellow diamonds stand for residues which were different between the two Cp149 constructs. Missing data points are due to missing assignments in either the solution-state (white circles) or the solid-state NMR study (grey circles). Secondary structure elements extracted from the X-ray structure are shown above the graph as pink boxes. Chemical shift differences below -1.5 ppm or above 1.5 ppm (grey dotted lines) are considered as significant. Three regions were identified and are colored in green, red, and blue. Isolated Met1 is highlighted in grey. **B)** Sphere representation of residues with significant chemical-shift differences between Cp149 dimer and Cp149 capsid. It includes residues M1, F18, L19, S21, D22, F23, L55, A58, L60, C61, W62, K96 and I97, which are labeled on subunit B and colored as in panel A. Residues N75 and L76 are not included, as the V74 to T74 substitution in the dimer in solution is likely to be at the origin of the observed CSPs. Helices are labeled on subunit A. PDB: 1QGT. The figures involving structures were all prepared using the PyMol software (Warren Delano, <http://www.pymol.org>).

Experiment	DARR	NCA	NCO	NCACB
------------	------	-----	-----	-------

Transfer 1	HC-CP	HN-CP	HN-CP	HN-CP
Field [kHz]	65.7(H)/50(C)	56.1(H)/43.1(N)	56.1(H)/43.1(N)	57.7(H)/43.1(N)
Shape	Tangent ¹ H	Tangent ¹ H	Tangent ¹ H	Tangent ¹ H
¹³ C carrier [ppm]	56.5			
time [ms]	1	0.9	0.9	0.9
Transfer 2	DARR	NCa-CP	NCO-CP	NCa-CP
Field [kHz]	17.5(H)	6(C)/10.9(N)	6(C)/11.5(N)	6(C)/11.5(N)
Shape	-	Tangent ¹³ C	Tangent ¹³ C	Tangent ¹³ C
¹³ C carrier [ppm]	97.8	54	174.9	59.9
time [ms]	20	6	6	6
Transfer 3				DREAM
Field [kHz]				8(C)
Shape				Tangent ¹³ C
Carrier [ppm]				56
time [ms]				3
t ₁ increments	2560	1344	1344	74
sw (t ₁) [kHz]	93.75	62.5	62.5	5.7
Acq. time (t ₁) [ms]	13.7	10.8	10.8	6.5
t ₂ increments	3072	2304	2304	120
sw (t ₂) [kHz]	93.8	100	100	8.0
Acq. time (t ₂) [ms]	16.4	11.5	11.5	7.5
t ₃ increments				2304
sw (t ₃) [kHz]				100
Acq. time (t ₃) [ms]				11.5
¹ H decoupling	SPINAL64	SPINAL64	SPINAL64	SPINAL64
Field [kHz]	90	90	90	90
Interscan delay d1 [s]	3	2.6	2.6	3
Number of scans	16	24	24	16
Measurement time	34 h	23 h	23 h	5 days

Experiment	NCACX	NCOCX	CANCO	CCC
Transfer 1	HN-CP	HN-CP	HC-CP	HC-CP
Field [kHz]	61.7(H)/43.1(N)	60.2(H)/43.1(N)	65.1(H)/50(C)	65.2(H)/50(C)
Shape	Tangent ¹ H	Tangent ¹ H	Tangent ¹ H	Tangent ¹ H
¹³ C carrier [ppm]				55
time [ms]	0.8	0.8	0.6	0.7
Transfer 2	NCa-CP	NCO-CP	CaN-CP	DREAM
Field [kHz]	6(C)/10.8(N)	6(C)/11.6(N)	6(C)/11.5(N)	8(C)
Shape	Tangent ¹³ C	Tangent ¹³ C	Tangent ¹³ C	Tangent ¹³ C
¹³ C carrier [ppm]	58.6	176.5	59.3	56
time [ms]	6.5	3	6.5	4
Transfer 3	DARR	DARR	NCO-CP	DARR
Field [kHz]	17.5(H)	17.5(H)	6(C)/10.9(N)	17.5(H)
Shape	-	-	Tangent ¹³ C	-
Carrier [ppm]	58.6	176.5	176.2	43.8
time [ms]	70	30	7	80
t ₁ increments	64	96	135	200

sw (t_1) [kHz]	5.7	5.7	8.0	15.1
Acq. time (t_1) [ms]	5.6	8.4	8.4	6.6
t_2 increments	85	108	100	200
sw (t_2) [kHz]	8.0	6.0	5.7	15.1
Acq. time (t_2) [ms]	5.3	9.0	8.8	6.6
t_3 increments	2304	2304	2304	2816
sw (t_3) [kHz]	100	100	100	93.75
Acq. time (t_3) [ms]	11.5	11.5	11.5	15.0
^1H decoupling	SPINAL64	SPINAL64	SPINAL64	SPINAL64
Field [kHz]	90	90	90	90
Interscan delay d1 [s]	2.9	3	3	2.75
Number of scans	16	16	8	4
Measurement time	3 days	6 days	4 days	5.2 days

Table 1. NMR experimental details. sw stands for spectral width. Experiments were recorded on an 800 MHz spectrometer at a 17.5 kHz MAS frequency and at a sample temperature of 5 °C. The ^{15}N -insert was removed from the probe for the CCC experiment to increase the signal to noise ratio.

Conclusion

The contribution of MAS-NMR spectroscopy to understanding structural and dynamical features of virus-like particles has become significant over the past years. Here we have shown that assembled hepatitis B virus capsids can be studied by solid-state NMR. This is of particular importance to further analyze the conformational dynamics the core protein is thought to undergo upon its multiple interactions with viral and cellular factors, both protein and nucleic acids, that eventually yield a mature infectious virion. Labeled Cp149 protein can be produced in pure form and in large quantity in *E. coli* and the protein yields high-quality spectra with narrow lines and a dispersion typical for an α -helical protein. Sequential assignments are to 87 % complete for Cp149 backbone, and yield secondary chemical shifts matching available X-ray structures of the capsid. Signals for residues downstream residue 140 are not detectable by either technique, owing to the dynamic behavior of the C-terminus, except for some core assembly mutants that are partially ordered down to residue 156 (Klumpp et al. 2015). However, a comparison with the solution-NMR chemical shifts

1 reported for the Cp149 dimer (Freund et al. 2008) highlights conformational differences in
2 three distinct regions of the protein, suggesting they are structurally affected by the transition
3
4 from the dimer state to the capsid state. In summary, the work presented here sets the stage
5
6 for future high resolution NMR studies of the HBV core protein which is central in HBV
7
8 infection and thus is also becoming a highly attractive target for novel anti-HBV therapeutics
9
10 (Zlotnick et al. 2015; Durantel and Zoulim 2016; Pei et al. 2017).
11
12
13
14
15

16 **Acknowledgements** This work was supported by the French ANR (ANR-14-CE09-0024B),
17
18 the LABEX ECOFECT (ANR-11-LABX-0048) within the Université de Lyon program
19
20 Investissements d'Avenir (ANR-11-IDEX-0007) (AB), the Swiss National Science
21
22 Foundation (Grant 200020_159707) (BHM), the DFG grant NA154/9-4 (MN), a doctoral
23
24 stipend from the Chinese Scientific Council (SW) and by the Marie Skłodowska-Curie
25
26 program (H2020-MSCA-IF-2016 748516) (LL). We thank the Centre d'Imagerie Quantitative
27
28
29
30
31
32
33
34
35
36
37
38
39
40
41
42
43
44
45
46
47
48
49
50
51
52
53
54
55
56
57
58
59
60
61
62
63
64
65

References

- 1
2 Abramov G, Morag O, Goldbourt A (2015) Magic-angle spinning NMR of intact bacteriophages: Insights into
3 the capsid, DNA and their interface. *Journal of Magnetic Resonance* 253:80–90. doi:
4 10.1016/j.jmr.2015.01.011
- 5
6 Andreas LB, Jaudzems K, Stanek J, et al (2016) Structure of fully protonated proteins by proton-detected magic-
7 angle spinning NMR. *Proc Natl Acad Sci USA* 113:9187–9192. doi: 10.1073/pnas.1602248113
- 8
9 Birnbaum F, Nassal M (1990) Hepatitis B virus nucleocapsid assembly: primary structure requirements in the
10 core protein. *Journal of Virology* 64:3319–3330.
- 11
12 Bourne CR, Finn MG, Zlotnick A (2006) Global Structural Changes in Hepatitis B Virus Capsids Induced by the
13 Assembly Effector HAP1. *Journal of Virology* 80:11055–11061. doi: 10.1128/JVI.00933-06
- 14
15 Böckmann A, Gardiennet C, Verel R, et al (2009) Characterization of different water pools in solid-state NMR
16 protein samples. *J Biomol NMR* 45:319–327. doi: 10.1007/s10858-009-9374-3
- 17
18 Böttcher B, Wynne SA, Crowther RA (1997) Determination of the fold of the core protein of hepatitis B virus by
19 electron cryomicroscopy. *Nature* 386:88–91. doi: 10.1038/386088a0
- 20
21 Chen C, Wang JC-Y, Zlotnick A (2011) A Kinase Chaperones Hepatitis B Virus Capsid Assembly and Captures
22 Capsid Dynamics in vitro. *PLoS Pathog* 7:e1002388–10. doi: 10.1371/journal.ppat.1002388
- 23
24 Conway JF, Cheng N, Zlotnick A, et al (1997) Visualization of a 4-helix bundle in the hepatitis B virus capsid
25 by cryo-electron microscopy. *Nature* 386:91–94. doi: 10.1038/386091a0
- 26
27 Crowther RA, Kiselev NA, Böttcher B, et al (1994) Three-dimensional structure of hepatitis B virus core
28 particles determined by electron cryomicroscopy. *Cell* 77:943–950.
- 29
30 Dryden KA, Wieland SF, Whitten-Bauer C, et al (2006) Native Hepatitis B Virions and Capsids Visualized by
31 Electron Cryomicroscopy. *Molecular Cell* 22:843–850. doi: 10.1016/j.molcel.2006.04.025
- 32
33 Durantel D, Zoulim F (2016) New antiviral targets for innovative treatment concepts for hepatitis B virus and
34 hepatitis delta virus. *Journal of Hepatology* 64:S117–S131. doi: 10.1016/j.jhep.2016.02.016
- 35
36 Freund SMV, Johnson CM, Jaulent AM, Ferguson N (2008) Moving towards High-Resolution Descriptions of
37 the Molecular Interactions and Structural Rearrangements of the Human Hepatitis B Core Protein. *Journal*
38 *of Molecular Biology* 384:1301–1313. doi: 10.1016/j.jmb.2008.10.020
- 39
40 Gallina A, Bonelli F, Zentilin L, et al (1989) A recombinant hepatitis B core antigen polypeptide with the
41 protamine-like domain deleted self-assembles into capsid particles but fails to bind nucleic acids. *Journal of*
42 *Virology* 63:4645–4652.
- 43
44 Habenstein B, Wasmer C, Bousset L, et al (2011) Extensive de novo solid-state NMR assignments of the 33 kDa
45 C-terminal domain of the Ure2 prion. *J Biomol NMR* 51:235–243. doi: 10.1007/s10858-011-9530-4
- 46
47 Han Y, Ahn J, Concel J, et al (2010) Solid-State NMR Studies of HIV-1 Capsid Protein Assemblies. *J Am Chem*
48 *Soc* 132:1976–1987. doi: 10.1021/ja908687k
- 49
50 Heger-Stevic J, Kolb P, Walker A, Nassal M (2017) Displaying whole-chain proteins on hepatitis B virus
51 capsid-like particles. *Virus-Derived Nanoparticles for Advanced Technologies*, in press
- 52
53 Katen SP, Tan Z, Chirapu SR, et al (2013) Assembly-Directed Antivirals Differentially Bind Quasiequivalent
54 Pockets to Modify Hepatitis B Virus Capsid Tertiary and Quaternary Structure. *Structure/Folding and*
55 *Design* 21:1406–1416. doi: 10.1016/j.str.2013.06.013
- 56
57 Klumpp K, Lam AM, Lukacs C, et al (2015) High-resolution crystal structure of a hepatitis B virus replication
58 inhibitor bound to the viral core protein. *Proc Natl Acad Sci USA* 112:15196–15201. doi:
59 10.1073/pnas.1513803112
- 60
61
62
63
64
65

- 1 Morag O, Abramov G, Goldbourn A (2014) Complete Chemical Shift Assignment of the ssDNA in the
2 Filamentous Bacteriophage fd Reports on Its Conformation and on Its Interface with the Capsid Shell. *J Am*
3 *Chem Soc* 136:2292–2301. doi: 10.1021/ja412178n
- 4 Nassal M (2015) HBV cccDNA: viral persistence reservoir and key obstacle for a cure of chronic hepatitis B.
5 *Gut* 64:1972. doi: 10.1136/gutjnl-2015-309809
- 6
7 Nassal M (1992) The arginine-rich domain of the hepatitis B virus core protein is required for pregenome
8 encapsidation and productive viral positive-strand DNA synthesis but not for virus assembly. *Journal of*
9 *Virology* 66:4107–4116.
- 10
11 Ning X, Basagoudanavar SH, Liu K, et al (2017) Capsid Phosphorylation State and Hepadnavirus Virion
12 Secretion. *Journal of Virology* 91:e00092–17–16. doi: 10.1128/JVI.00092-17
- 13
14 Patel N, White SJ, Thompson RF, et al (2017) HBV RNA pre-genome encodes specific motifs that mediate
15 interactions with the viral core protein that promote nucleocapsid assembly. *Nature Microbiology* 1–10.
16 doi: 10.1038/nmicrobiol.2017.98
- 17
18 Pei Y, Wang C, Yan SF, Liu G (2017) Past, Current, and Future Developments of Therapeutic Agents for
19 Treatment of Chronic Hepatitis B Virus Infection. *J Med Chem* acs.jmedchem.6b01442–19. doi:
20 10.1021/acs.jmedchem.6b01442
- 21
22 Penzel S, Smith AA, Agarwal V, et al (2015) Protein resonance assignment at MAS frequencies approaching
23 100 kHz: a quantitative comparison of J-coupling and dipolar-coupling-based transfer methods. *J Biomol*
24 *NMR* 1–22. doi: 10.1007/s10858-015-9975-y
- 25
26 Quinn CM, Lu M, Suiter CL, et al (2015) Magic angle spinning NMR of viruses. *Progress in Nuclear Magnetic*
27 *Resonance Spectroscopy* 86-87:21–40. doi: 10.1016/j.pnmrs.2015.02.003
- 28
29 Revill P, Testoni B, Locarnini S, Zoulim F (2016) Global strategies are required to cure and eliminate HBV
30 infection. *Nature Reviews Gastroenterology And Hepatology* 13:239–248. doi: 10.1038/nrgastro.2016.7
- 31
32 Schuetz A, Wasmer C, Habenstein B, et al (2010) Protocols for the Sequential Solid-State NMR Spectroscopic
33 Assignment of a Uniformly Labeled 25 kDa Protein: HET-s(1-227). *Chem Eur J of Chem Bio* 11:1543–
34 1551. doi: 10.1002/cbic.201000124
- 35
36 Selzer L, Kant R, Wang JCY, et al (2015) Hepatitis B Virus Core Protein Phosphorylation Sites Affect Capsid
37 Stability and Transient Exposure of the C-terminal Domain. *J Biol Chem* 290:28584–28593. doi:
38 10.1074/jbc.M115.678441
- 39
40 Stanek J, Andreas LB, Jaudzems K, et al (2016) NMR Spectroscopic Assignment of Backbone and Side-Chain
41 Protons in Fully Protonated Proteins: Microcrystals, Sedimented Assemblies, and Amyloid Fibrils. *Angew*
42 *Chem* 128:15730–15735. doi: 10.1002/ange.201607084
- 43
44 Stevens TJ, Fogh RH, Boucher W, et al (2011) A software framework for analysing solid-state MAS NMR data.
45 *J Biomol NMR* 51:437–447. doi: 10.1007/s10858-011-9569-2
- 46
47 Suiter CL, Quinn CM, Lu M, et al (2015) MAS NMR of HIV-1 protein assemblies. *Journal of Magnetic*
48 *Resonance* 253:10–22. doi: 10.1016/j.jmr.2014.12.009
- 49
50 Vranken WF, Boucher W, Stevens TJ, et al (2005) The CCPN data model for NMR spectroscopy: development
51 of a software pipeline. *Proteins* 59:687–696. doi: 10.1002/prot.20449
- 52
53 Wishart DS, Bigam CG, Holm A, et al (1995) ¹H, ¹³C and ¹⁵N random coil NMR chemical shifts of the
54 common amino acids. I. Investigations of nearest-neighbor effects. *J Biomol NMR* 5:67–81.
- 55
56
57 World Health Organization (2017) Global hepatitis report. In: www.who.int. Apr 2017
- 58
59 Wynne SA, Crowther RA, Leslie AG (1999) The crystal structure of the human hepatitis B virus capsid.
60 *Molecular Cell* 3:771–780.
- 61
62
63
64
65

1 Yu X, Jin L, Jih J, et al (2013) 3.5 Å cryo-EM Structure of Hepatitis B Virus Core Assembled from Full-Length
2 Core Protein. PLoS ONE 8:e69729–11. doi: 10.1371/journal.pone.0069729

3 Zlotnick A, Venkatakrishnan B, Tan Z, et al (2015) Core protein: A pleiotropic keystone in the HBV lifecycle.
4 Antiviral Research 121:82–93. doi: 10.1016/j.antiviral.2015.06.020

5
6 Zoulim F, Durantel D (2015) Antiviral Therapies and Prospects for a Cure of Chronic Hepatitis B. Cold Spring
7 Harbor Perspectives in Medicine 5:a021501–a021501. doi: 10.1101/cshperspect.a021501
8
9

10
11
12
13
14
15
16
17
18
19
20
21
22
23
24
25
26
27
28
29
30
31
32
33
34
35
36
37
38
39
40
41
42
43
44
45
46
47
48
49
50
51
52
53
54
55
56
57
58
59
60
61
62
63
64
65